analytical chemistry

pubs.acs.org/ac Article

Isothermal Background-Free Nucleic Acid Quantification by a One-Pot Cas13a Assay Using Droplet Microfluidics

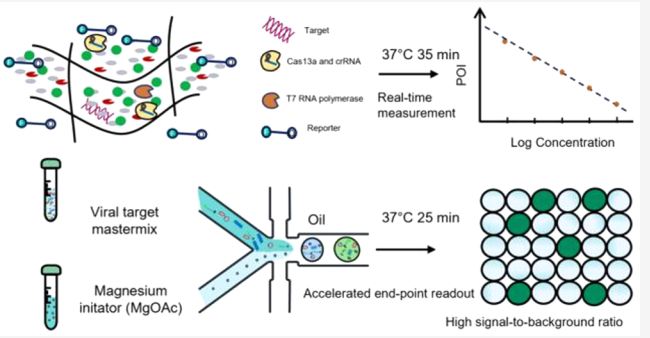
Frank X. Liu,[¶] Johnson Q. Cui,[¶] Hojeong Park,[¶] Ka Wai Chan, Tyler Leung, Ben Zhong Tang,* and Shuhuai Yao*

Cite This: https://doi.org/10.1021/acs.analchem.2c00067 Read Online

ACCESS | Metrics & More | Article Recommendations | Supporting Information

Downloaded via SHANGHAI NORMAL UNIV on April 12, 2022 at 07:38:01 (UTC).
See https://pubs.acs.org/sharingguidelines for options on how to legitimately share published articles.

ABSTRACT: High sensitivity and specificity nucleic acid detection has been achieved by the Cas13a collateral effect in combination with a separate recombinase polymerase amplification (RPA). However, these emerging methods cannot provide accurate quantification of nucleic acids because the two-step assay performance may be compromised if the RPA and Cas13a reactions are simply unified in a single step. In this work, we first addressed the challenges associated with enzymatic incompatibility and the macromolecular crowding effect in the one-pot assay development, making the consolidated RPA-Cas13a assay a facile and robust diagnostic tool. Next, we found that the one-pot reaction cannot precisely quantify the targets at low concentrations. Thus, by leveraging droplet microfluidics, we converted the one-pot assay to a digital quantification format, termed Microfluidics-Enabled Digital Isothermal Cas13a Assay (MEDICA). Due to the droplet compartmentation, MEDICA greatly accelerates the reaction and enables relative detection in 10 min and the end-point quantification in 25 min. Moreover, MEDICA facilitates the droplet binarization for counting because of background-free signals generated by trans-cleavage reporting of Cas13a. Our clinical validation highlights that CRISPR-based isothermal assays are promising for the next generation of nucleic acid quantification methods.



INTRODUCTION

Rapid, robust, and inexpensive diagnostics are crucial in defense against the spread of viral infections such as SARS-CoV, MERS-CoV, Ebola, Zika, avian, and swine influenza. The COVID-19 pandemic highlights the unprecedented demand for rapid and sensitive nucleic acid detection assays, which play a pivotal role in routine diagnosis, mechanistic and transmission studies, vaccine development, and therapeutics for COVID-19.[1] Quantitative polymerase chain reaction (qPCR) has long been regarded as a gold standard for viral infection diagnosis.[2,3] However, as a centralized laboratory-based testing paradigm for viral diagnostics, PCR assays depend on specifically designed TaqMan probes as well as precise thermal cycling, limiting their deployability for community tests.

Recently, clustered regularly interspaced short palindromic repeats (CRISPR) and CRISPR-associated endonucleases are leveraged for nucleic acid detection through unique collateral trans-cleavage.[4−10] Programmable crRNA-guided CRISPR Cas12 and Cas13 can specifically recognize the target sequence to promote trans cleavage of surrounded single-stranded reporters.[11,12] Combined with a separate step of isothermal recombinase polymerase amplification (RPA) preamplification, Cas13a based SHERLOCK (Specific High-sensitivity Enzymatic Reporter unlocking) and Cas12a based DETECTR (DNA endonuclease-targeted CRISPR trans reporter) assays achieved attomolar sensitivity and single nucleotide polymorphism (SNP) identification ability.[13,14] Due to the strong collateral reporting,[8,15,16] the two-step SHERLOCK assay even pushed the limit of detection (LOD) to the single-molecule level.

Currently, most state-of-the-art diagnostic platforms with CRISPR detection use fluorescence or strip tests to visualize a yes-or-no result[5,8,10,13,17,18] but fail to provide quantitative measurement that is essential for monitoring responses to treatment and fundamental biological research.[19,20] Quantitative methods including real-time or end-point quantification require a robust and sensitive one-pot reaction (e.g., PCR). Separating the amplification and detection into two steps not only imposes difficulties for integrated workflow but also makes quantification of the original target concentration inaccurate. Therefore, a robust and reproducible one-pot

Received: January 6, 2022
Accepted: March 24, 2022

© XXXX American Chemical Society

reaction is a prerequisite for nucleic acid quantification using RPA and Cas13a.

Recently, the one-pot SHERLOCK assay has been developed to detect COVID-19 using a dipstick test and fluorescence measurement.[18] A similar result was reported in another work using RPA-based Cas12a.[7] However, significant signal differences in different aliquoted groups have been shown from these assays, which may lead to false-negative results. One hypothesis of such results is the issue associated with the high molecular weight polyethylene glycol (PEG),[21,22] which is an important component in RPA formulation as a crowding agent.[23] Crowding agents have been shown to regulate the efficiency of various biochemical processes, including enhanced enzyme catalytic activity.[24,25] However, for RPA that operates at a relatively low temperature, the high activity of the RPA reaction would cause the local reagent depletion, suppressing the cascade of the subsequent reactions.[26] When the Cas13a system is introduced into the RPA based reaction, the Cas13a reaction for detection would be inevitably affected due to the local depletion of reagents without proper diffusion or mixing. In addition, the multiple-enzyme reactions in the one-pot assay of RPA and Cas13a have to be compatible in a mixture. Therefore, the macromolecular crowding and enzymatic incompatibility issues must be addressed in order to make the one-pot assay achieve a comparable performance of the two-step SHERLOCK system.

In this work, we first combine RPA reaction and Cas13a detection into a one-pot assay to achieve sensitive and robust quantification of nucleic acids. To identify the optimal assay condition, we systematically investigated the effects of different components such as reaction buffer, enzymes, PEG, and other additives. We found that appropriately reducing the concentration of PEG-8000 can improve the reproducibility of the one-pot reaction because the crowding effect is alleviated. After full optimization, the one-pot RPA-Cas13a assay is applied for real-time quantification. Furthermore, we convert this one-pot assay into water-in-oil droplets for digital quantification. This method, termed Microfluidics-Enabled Digital Isothermal Cas13a Assay (MEDICA), enables background-free binarization of droplets where the signals are only triggered by the trans reporting of Cas13a in the presence of the desired targets. We demonstrated that MEDICA achieved qualitative detection within 10 min and quantitative detection within 25 min, owing to the droplet confinement where the reaction is greatly enhanced. Lastly, we applied MEDICA for the clinical diagnosis of HPV 16 and HPV 18, indicating complete accordance with qPCR results.

MATERIALS AND METHODS

Chemicals and Sequences. Detailed information about reagents, including the commercial vendors and stock concentrations, all chemicals, and sequences related to this work are listed in Tables S4 and S5.

LwaCas13a Protein Extraction. *E. coli* Rosetta 2(DE3) pLysS was transformed with the pC013 TwinStrep-SUMO-huLwaCas13a (Addgene plasmid no. 90097).[22] The cells were cultured at 37 °C in 15 mL of Luria−Bertani (LB) medium containing ampicillin overnight. A volume of 5 mL of overnight cultures were added into 1 L of LB medium containing ampicillin and allowed to grow at 37 °C. When the OD_{600} reached 0.4−0.6, the cultures were cooled down at 4 °C for 30 min before the protein induction. The cultures were grown at 16 °C for 18 h with ampicillin and 0.1 mM IPTG. Cells were collected, resuspended in 4× (wt/vol) supplemented lysis buffer (20 mM pH 8.0 Tris-HCl, 0.5 M NaCl, 1 mM DTT, 2 cOmplete Ultra EDTA-free tablets, 100 mg of lysozyme, and 1 μL of benzonase in 60 mL of lysis buffer) and ruptured on ice by sonication (Q500, QSONICA). The lysate was centrifuged at 4 °C for 60 min at 10 000 rpm and the supernatant was incubated with 0.5 mL of Strep-Tactin superflow Plus resin for 3 h by gentle shaking at 4 °C. The resin-sample suspension was poured into 50 mL of Bio-Rad glass Econo-Column equilibrated with cold lysis buffer. After discarding flow-through, 5 mL of SUMO protease cleavage solution composed of 5 mL of lysis buffer, 50 μL of SUMO protease, and 7.5 μL of NP-40 was added to the column, followed by gentle shaking at 4 °C overnight. The collected cleavage solution was dialyzed in 2 L of PBS in a cellulose membrane dialysis tube at 4 °C overnight. The presence of recombinant was identified using SDS-PAGE gel analysis (Figure S1). Amicon Ultra-0.5 mL centrifugal filter was used to concentrate protein and rediluted in protein storage buffer, which allows the protein for storage at −80 °C.

Clinical Extraction and qPCR Validation. Clinical swab samples were provided by DiagCor Bioscience from clinical doctors in compliance with ethical and safety approval (HREP-2021-0161) by the Human Research Ethics Committee and Health, Safety and Environment Office of HKUST.

We used QIAamp DNA Mini Kit (Qiagen) to extract the viral RNAs according to the manufacturer's protocol. The raw urine sample is 10 mL each. After extraction, samples were collected with a 1.5 mL tube and stored at −20 °C before use.

The qPCR was performed with a master mix of 20 μL including 10 μL of 2× Taq polymerase, 0.5 μL of 10 μM forward and reverse primers each, 0.5 μL of 10 μM probes, 5.5 μL of nuclease-free water, and 2 μL of target sample from the extraction. After gentle mixing, the two-step PCR was conducted with 30 s preheating followed by 45 cycles of 5 s at 95 °C (denaturation) and 30 s at 60 °C (annealing and extension). All the qPCR experiments were conducted with a Roche Lightcycler 480 II (Roche) at HKUST BioCRF.

SHERLOCK Assays. The standard SHERLOCK includes two steps. First, the RPA preamplification was triggered by adding MgOAc from the kit instructed with TwistAmp Basic at 37 °C for 20 min. Second, 1 μL of the RPA product was added to 19 μL of Cas13a detection master mix consisting of 20 mM HEPES (pH 6.8), 9 mM $MgCl_2$, 1 mM rNTP mix, 40 nM LwaCas13a, 1 U/μL RNase inhibitor murine, 0.125 U/μL T7 RNA polymerase, and 125 nM poly(U) RNA reporters. The sample was incubated with a Roche Lightcycler 480 II (Roche) at 37 °C, and the fluorescence signals were measured every minute for 1 h.

Buffer Construction and Optimization for One-Pot Assay. The optimization of components of the RPA and Cas13a reaction started with an initial reaction including 1× buffer containing 50 mM Tris-HCl (pH 8.0), 60 mM NaCl, 5% PEG-8000, and 2 mM DTT. The initial master mix was created with 100 nM Cas13a, 1 mM rNTP mix, 10 U of RNase inhibitor Murine, 100 nM crRNA, 5U of T7 RNA polymerase, 125 nM PolyU reporters, and 480 nM of each forward and reverse primers, and one lyophilized pellet from the basic RPA kit. In all experiments, the master mix without MgOAc was used to suspend the lyophilized pellet (one pellet to 100 μL final reaction volume). After reconstitution, this master mix was aliquoted accordingly, with each group containing 17 μL of reconstituted master mix. Then, 2 μL of the synthetic

https://doi.org/10.1021/acs.analchem.2c00067
Anal. Chem. XXXX, XXX, XXX−XXX

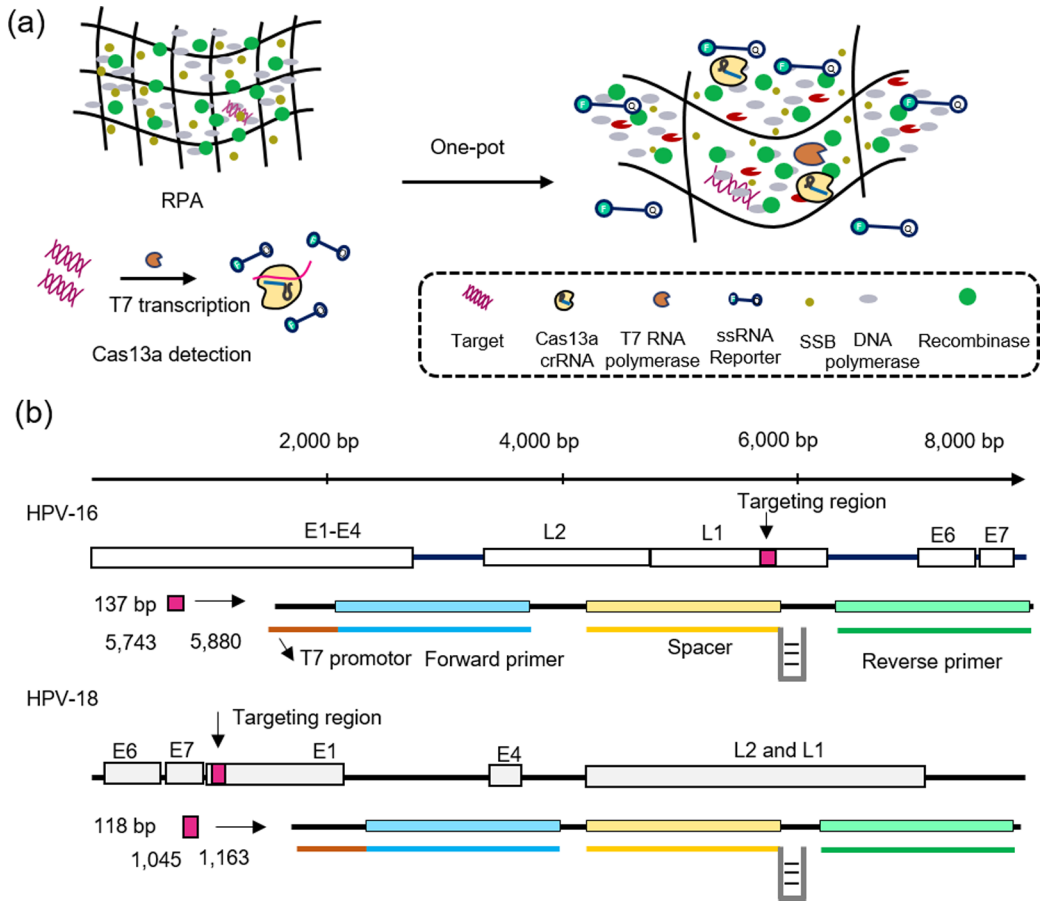


Figure 1. Overview of viral HPV 16 and HPV 18 quantification with one-pot Cas13a. (a) The RPA reaction and Cas13a detection are unified into a one-pot assay by alleviating the potential interferences that arise from the crowding agent and mediating the effects of various types of enzymes. (b) Genome map of both HPV 16 and HPV 18. The selected detection regions of HPV 16 L1 and HPV 18 E1 are annotated with red lines in the genome, which covers the forward RPA primer with the extended T7 region overhang, targeted protospacer, and reverse primer. The targeted HPV 16 region has 137 bp (from 5743 bp to 5880 bp) while the HPV 18 detection region has 118 bp (from 1045 bp to 1163 bp). Spacer represents the crRNA spacer.

sample or viral specimen was pipetted into this master mix with thorough mixing. Finally, 1 μL of MgOAc (280 mM) from the kit was added to trigger this reaction.

Then optimization occurred iteratively with each reagent modification. We identified each component to yield the best signal and then kept the optimal reagent tested previously when conducting the next optimization. We evaluated the performance of Tris-HCl with different concentrations (10, 20, 40, 60, 80, and 100 mM) as well as pH (6.8, 7.5, and 8.0). For the salt components, we tested $NH_4(SO_4)_2$, NaCl, KCl, and CH_3COOK at different concentrations (20, 60, and 80 mM), respectively. Then, we optimized the PEG-8000 concentration (0, 2.5, 5, and 7.5%). For the additives, we tested the Tween 20 (0, 0.05, 0.1, 0.2, and 0.5%). After the buffer construction, we further optimized primer concentration (60, 120, 240, 360, and 480 nM), crRNA to Cas13a ratio (0, 0.5, 1, 2, 3, and 3.75), and T7 polymerase (0, 0.1, 0.4, 0.8, and 2 U/μL), respectively. All the modulated reaction components are shown in the figures and associated figure captions.

One-Pot Cas13a Assay for Nucleic Acid Detection. The optimized one-pot assay contains 1× reaction buffer (60 mM Tris-HCl pH 7.5, 80 mM KCl, 2.5% PEG-8000, 0.05% Tween 20, and 1 mM DTT), 40 nM Cas13a, 1 mM rNTP mix, 10 U Rnase inhibitor Murine, 40 nM crRNA, 0.8 U/μL T7 RNA polymerase, 125 nM Poly(U) reporters, and 360 nM each forward and reverse primers, and the enzymes from the lyophilized pellet (one pellet to 100 μL of final master mix including the target). Once the master mix is created, it is used to resuspend the lyophilized pellets. The final reaction volume is 20 μL containing 17 μL of aliquoted master mix, 2 μL of target sample, and 1 μL of MgOAc.

We further evaluated the performance of the sensitivity, specificity, and comparison of the one-pot reaction. All the experiments were conducted in real-time with the Roch Lightcycler 480 II with fluorescence measurement every minute at 37 °C for 1 h. For the specificity test, the spiked genes were first prepared at 1×10^5 cp/μL and mixed mutually before experiments.

Droplet Microfluidic Device Design and Fabrication. The microfluidic device consists of Y-shaped two inlets for MgOAc and target-included master mix, respectively, and two symmetric oil channels (fluorinated oil 7500 with 2.5% EA surfactant) to form a flow-focusing droplet generator. The thickness of the device is 35 μm, and all the inlets are 40 μm until the flow-focusing junction with tiny modification. The aqueous phase channel of the junction is 30 μm while the oil channel is 25 μm. The outlet channel is 100 μm until the end.

The device was made of polydimethylsiloxane (PDMS, Sylgard 184 silicone elastomer, Dow Corning) using a standard soft lithography process. A silicon master was first fabricated

https://doi.org/10.1021/acs.analchem.2c00067
Anal. Chem. XXXX, XXX, XXX−XXX

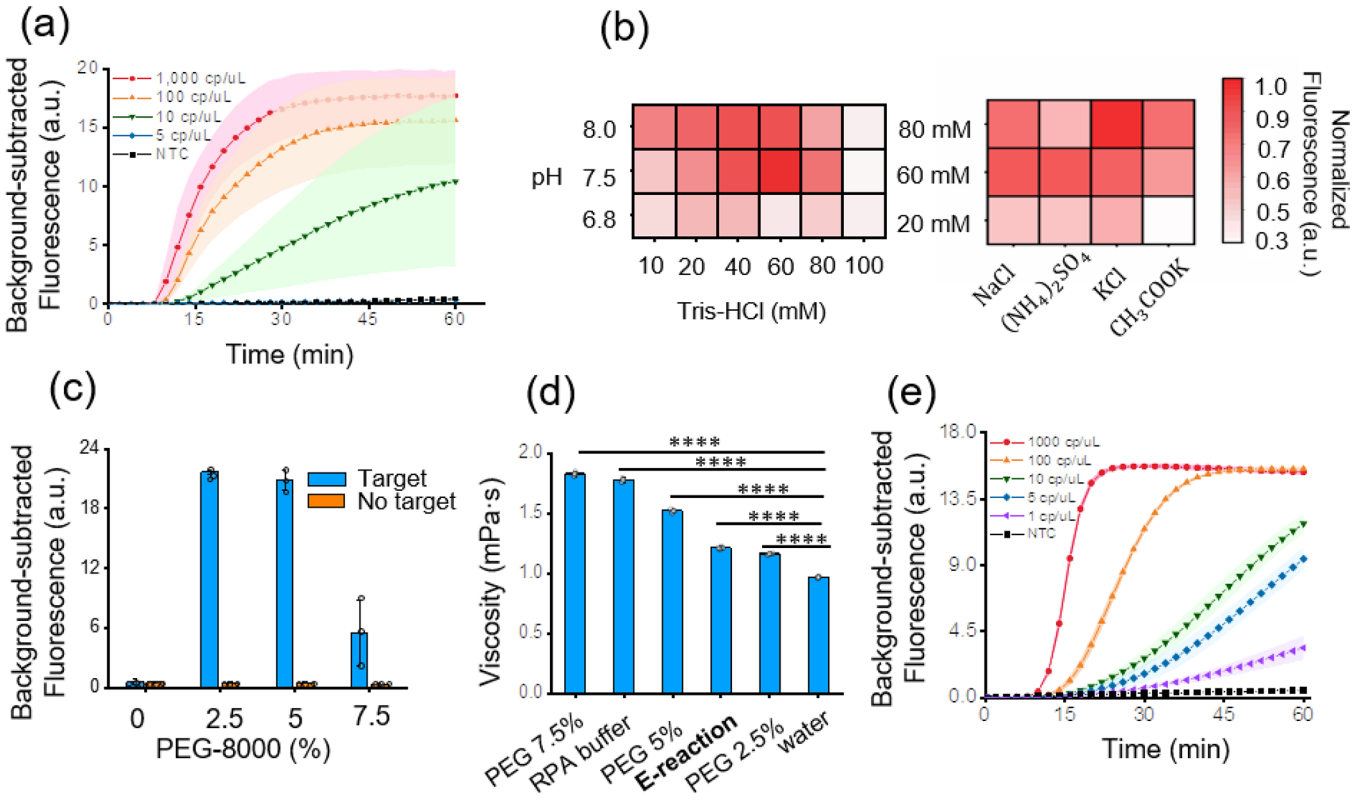


Figure 2. Construction and evaluation of the one-pot reaction. (a) The dilution of the initial one-pot reaction shows a wide range of fluorescence variations and limited sensitivity to detect the synthetic HPV 16 plasmid from 1000 cP/μL to 5 cP/μL, where the 5 cP/μL is not detectable. (b) The pH and salt optimization for the one-pot reaction. Tris-HCl of pH 6.8, 7.5, 8, and different concentrations are compared. Sodium chloride (NaCl), amino sulfate ($(NH_4)_2SO_4$), potassium chloride (KCl), and potassium acetate (CH_3COOK) of different concentrations are compared. (c) PEG-8000 of 0, 2.5, 5, and 7.5% was compared. (d) Viscosity comparison of different reaction conditions using different concentrations of PEG-8000; the E-reaction buffer represents the optimal reaction buffer. (e) The real-time fluorescence of the optimized one-pot assay for detection of a serial dilution of HPV 16 plasmid from 1000 cP/μL to 1 cP/μL. For parts a and e, the filled area represents the error bar (s.d.) of each group. For parts c and d, the center is the mean of three technical replicates, while the error bar indicates the standard deviation (s.d.) For part d, the two-tailed student's *t* test; ****$P < 0.0001$. For parts b and c, the concentration of plasmid HPV 16 is 10 cP/μL. The NTC represents the nontemplate control.

for PDMS replica molding. Microchannels were formed by bonding the PDMS to a glass substrate via oxygen plasma treatment. The microchannels were rendered hydrophobic after being treated with Aquapel.

MEDICA Data Acquisition and Quantification. The experiment was conducted with a pressure box (Everflow) to control the three phases (magnesium phase, master mix with target, and oil phase). The total reaction volume is 20 μL containing two phases with equal volumes. The 10 μL of magnesium phase contains 1× reaction buffer, 28 mM MgOAc. The volume of 10 μL of the other phase includes 1× enhanced reaction buffer, 80 nM Cas13a, 2 mM rNTP, 16 U of Rnase inhibitor Murine, 80 nM crRNA, 1.6 U/μL T7 polymerase, 720 nM each forward and reverse primers, 1 μM poly(U) reporters, and 2 μL of 1× target sample.

For end-point MEDICA, after 30 min incubation at 37 °C, droplets were pipetted into a 30 μm thick microchamber for fluorescence imaging. For the real-time MEDICA, first a heating system with a Peltier on microscopy was made with a PMMA frame. The temperature was calibrated to 37 °C. The sample was partitioned and then collected on ice. Then, all the droplets were pipetted into a silicon chamber (30 μm in depth) on ice. The inlet and outlet were sealed with optical adhesive film (Thermo Fisher). The time (0) image was recorded without heating. Then, the heating source was opened to record the fluorescence signal evolving with time. We used the synthetic SARS-CoV-2 ORF plasmid as an example to measure the real-time fluorescence change. The master mix was prepared with 1 × 10^5cp/μL target input, following the same protocol as MEDICA. The amplification time (Cq) for classifying samples as positive or negative was set to approximately 10% of the average steady-state fluorescence signal.

The droplet imaging system includes a LED light source with a 488 nm filter and a Nikon microscope (Eclipse Ti2) coupled with a sCMOS camera (ANDOR, Oxford Instruments). All the information (number and fluorescence intensity) was calculated by ImageJ (NIH). The detailed process of image analysis is listed in Figure S8. According to the Poisson law, the average number of target DNA per droplet λ was calculated through the possibility of positive droplets ($p_{postive}$). Let M be the total number of droplets and $V_{droplet}$ the average droplet volume. The molar concentration of the target n, can be

$$\lambda = -\ln(1 - p_{positive}) \quad (1)$$

$$n = \frac{\lambda}{V_{droplet}} \quad (2)$$

https://doi.org/10.1021/acs.analchem.2c00067
Anal. Chem. XXXX, XXX, XXX−XXX

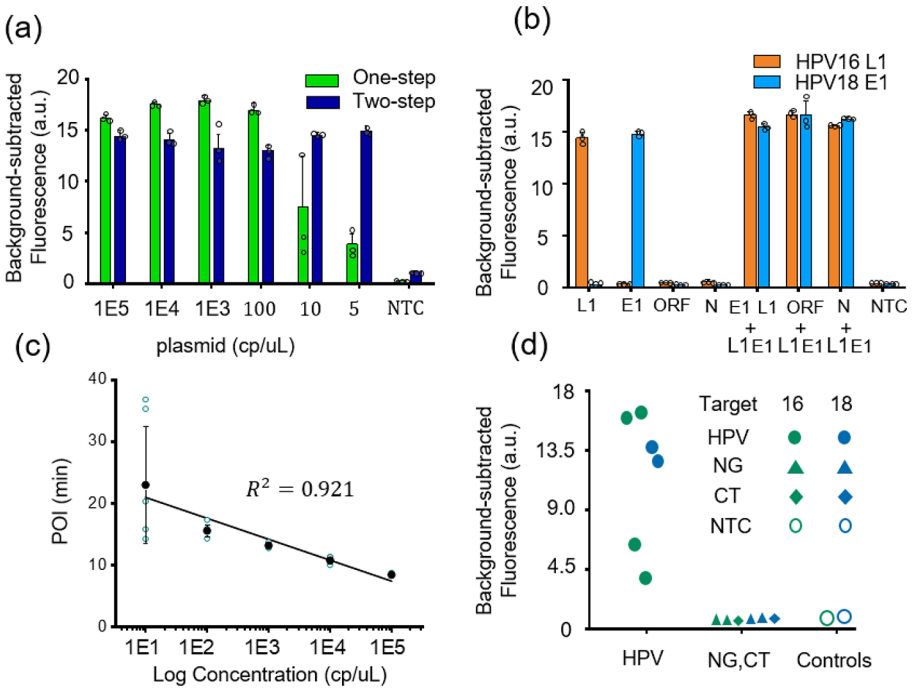


Figure 3. Performance evaluation of the optimized one-pot Cas13a assay. (a) The comparison of two-step and the optimized one-pot assay after 1 h using HPV 16 plasmid. (b) Specificity of the one-step assay with or without spiked plasmid targets. ORF and N indicate the SARS-CoV-2 ORF gene and N gene, respectively. (c) Standard curve for relative quantification from 10 cP/μL to 100 000 cP/μL. Each color represents a one-group experiment at various concentrations (The experiment was repeated six times). (d) Clinical validation of the one-pot assay. HPV 16, HPV 18, NG, and CT samples were tested to verify the one-pot assay performance. The green color group represents the HPV 16 detection while the blue group shows the HPV 18 diagnosis. For parts a–c, the center is the mean of the replicates, while the error bar indicates the s.d. The NTC represents the nontemplate control.

RESULTS AND DISCUSSION

One-Pot Nucleic Acid Cas13a Assay for Viral Detection. The multistep schemes not only increase the risk of contamination and sample loss in detection but also make the quantification of the target molecules difficult or inaccurate. We design a combined one-pot reaction scheme that uses RPA as preamplification and Cas13a as the collateral effect to allow facile detection and robust quantification (Figure 1a). Different from PCR that relies on thermocycles to denature and amply the target DNAs, RPA is performed using enzymatic activity to drive amplification isothermally (e.g., at temperatures of 37–42 °C). The RPA process employs a cocktail of recombinase enzymes, single-stranded DNA-binding proteins (SSBs), and DNA enzymes to achieve double-stranded DNA denaturation and strand invasion in the presence of a crowding agent (e.g., PEG).[23] Meanwhile, the Cas13a detection starts from T7 RNA transcription to Cas13a trans-cleavage of the neighboring ssRNA reporters. The one-pot reaction is developed to address the multienzyme reaction while balancing the crowding reaction influence between RPA amplification and trans-reporting of Cas13a. Since HPV is critical for identifying the risk of HPV-related cancers such as cervical cancer, HPV 16 and HPV 18 are accounted for the most precancerous lesions among all HPV types.[27] We designed two sets of RPA and Cas13a sequences that include forward primers with an overhanging T7 promoter, Cas13a crRNAs to recognize both HPV 16 and HPV 18 for specific and sensitive tests (Figure 1b) to validate the clinical diagnostic performance of the developed one-pot Cas13a reaction for nucleic acid quantification.

One-Pot Cas13a Assay Development. When we conducted the one-pot assay combining all the reagents used in the SHERLOCK,[8] we found the results had dramatic fluctuations and poor sensitivity compared to the two-step approaches (Figure 2a, Figure S2). The signal variability in each iterative experiment indicated irreproducible results, which may lead to false-negative results. Besides, this one-pot reaction failed to yield detectable signals below 5 cP/μL while the SHERLOCK showed single-molecule resolution (Figure S2). The compromised sensitivity and irreproducibility are likely caused by the reaction component incompatibility and high viscous crowding agent.[21,22] To reconcile enzymatic incompatibility, we performed multiple rounds of assay optimization to identify the key factors affecting the combined reaction. First, we investigated the components of the reaction buffer including pHs, salts, and other additives. We found the 60 mM pH 7.5 Tris-HCl buffer with 80 mM KCl yielded the highest signal, much better than the HEPES buffer used for the one-pot RPA and Cas13a (Figure 2b and Figure S3a). Subsequently, we investigated the crowding agent influence. This issue is originated from the high molecular weight PEG which hinders the movement of other molecules such as T7 polymerase, Cas13a nuclease, crRNA, and reporters and thus affecting the trans-cleavage of reporters before or after CRISPR ternary activation. PEG of high concentrations is widely applied to enhance the enzymatic activity, e.g., in the PCR system.[25] For the hot-start PCR, the molecular diffusion can be enhanced at a high-temperature condition even with highly viscous PEG. However, for RPA that operates at a near-ambient temperature, the molecular diffusion is hindered by the macromolecular crowding effect of PEG. Besides, the fast

https://doi.org/10.1021/acs.analchem.2c00067
Anal. Chem. XXXX, XXX, XXX−XXX

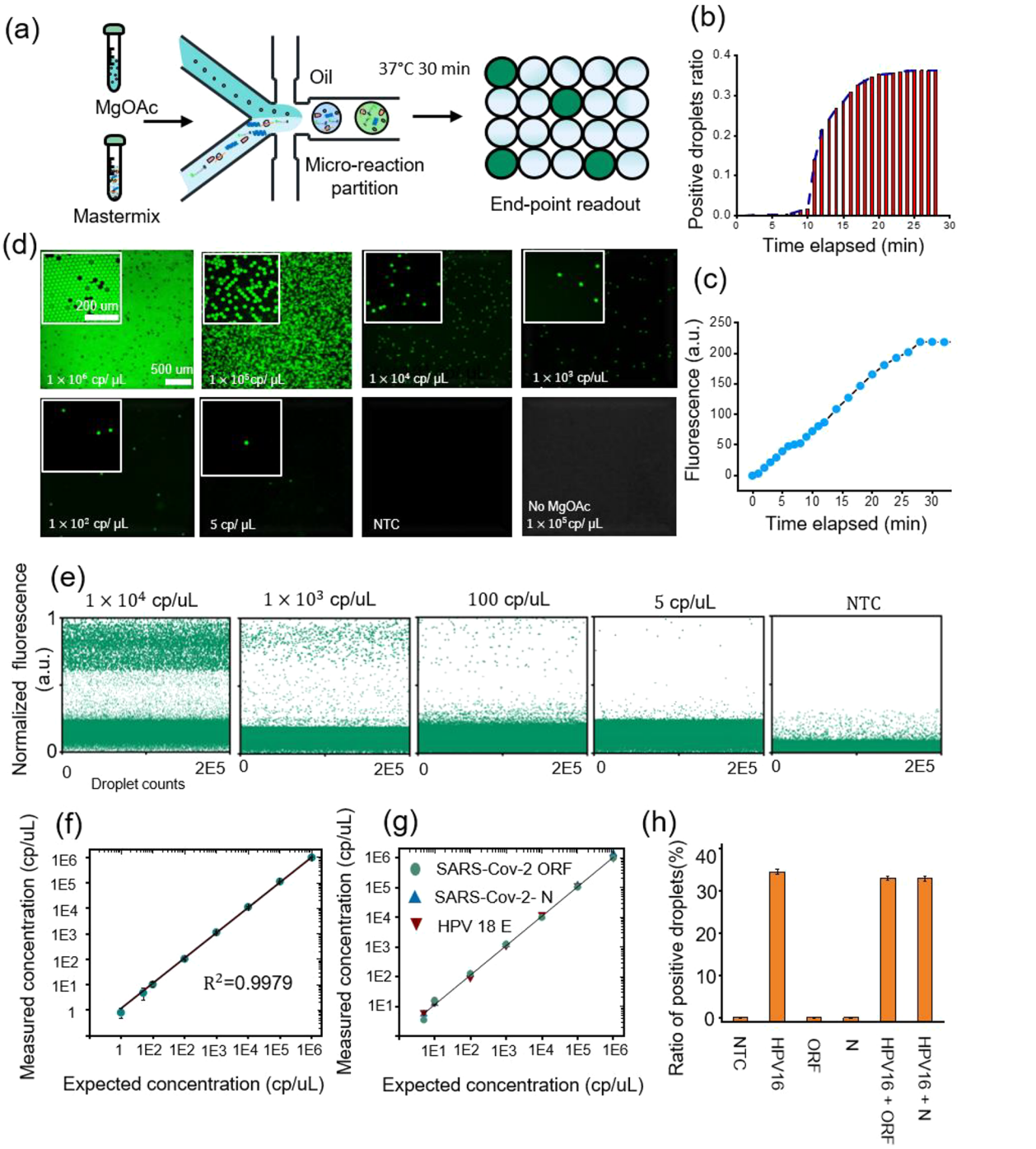


Figure 4. Real-time and end-point MEDICA: (a) workflow of the microfluidics-enabled digital isothermal Cas13a assay (MEDICA), which includes sample and initiator separation, droplet compartmentation, and visualization. (b) The percentage of positive droplet ratio along the reaction time. A time of 10 min was the turnover point for qualitative detection, and the ratio was saturated around 25 min. (c) The average intensity of all droplets over the reaction time. The highest fluorescence was yielded around 25 min. (d) The fluorescence images of the end-point MEDICA using a serial dilution of the sample ranging from 1×10^6 cp/μL to NTC. The extra control group was 1×10^5 cp/μL with the absence of the MgOAc initiator. (e) The statistical analysis of the end-point results. (f) The measured concentration is in excellent agreement with the expected concentration of HPV 16 plasmid, error bars represent s.d. (g) Quantification of the SARS-CoV-2 ORF gene, SARS-CoV-2 N gene, and HPV 18 N gene by MEDICA. (h) Selectivity test of MEDICA to target HPV 16 with or without spiked into ORF and N gene groups. The concentration was 1×10^5 cp/μL. Error bars represent the 95% confidence interval.

RPA reaction depletes the local reagents quickly, thus causing the overall reaction inhomogeneous and irreproducible. We then investigated the influence caused by PEG-8000 in the combined RPA and Cas13a reaction (Figure 2c). As the concentration of PEG-8000 increased over 5%, the fluorescence signal of the one-pot reaction fluctuated significantly. We reduced the PEG-8000 concentration to 2.5%, the signal fluctuations caused by inhomogeneous molecule distribution were greatly eased while maintaining robust detection performance. Moreover, we added 0.05% tween 20, a

https://doi.org/10.1021/acs.analchem.2c00067
Anal. Chem. XXXX, XXX, XXX−XXX

surfactant commonly used in droplet microfluidics,[28] to reduce the viscosity even further (Figure S3b).

We compared the viscosity of the enhanced reaction buffer (E-reaction) with other PEG-based reaction buffers (Figure 2d). The optimal one-pot reaction buffer is less viscous than most of the other PEG-based reaction buffers. These improvements decrease the viscosity of the reaction buffer; in another word, the molecule diffusion ability is increased at a lower temperature. To further enhance the detection ability, we optimized the primer concentration for the one-pot reaction (Figure S3c). The 120 nM and 360 nM primers resulted in a strong fluorescence signal and 360 nM primers performed better at 10 cP/μL concentration (Figure S3d). Besides, we optimized all the other related components including the crRNA to Cas13a ratio and the concentration of T7 polymerase (Figure S3e,f). Compared to the initial one-pot reaction, both sensitivity and reproducibility are improved (Figure 2e, Figures S4 and S5), where the optimized one-pot reaction can detect a single copy per microliter with high robustness.

Performance Evaluation and Clinical Validation of the Optimized One-Pot Cas13a Assay. We evaluated the performance of the optimized one-pot Cas13a reaction. The optimized assay indicated consistent detection ability down to 5 cP/μL (Figure 3a). Then we conducted the specificity of the assay to detect HPV16 and HPV18. Four synthetic plasmids containing HPV 16 L1 gene, HPV 18 E1 gene, SAR-CoV-2 ORF gene, and SAR-CoV-2 N gene were applied. We spiked the targeted HPV 16 into the unrelated samples to compare the performance inside the complicated matrix. The optimized one-pot Cas13a assay achieved high specificity, as shown in Figure 3b, and only the samples with the presence of the desired targets yielded significant signals.

In Figure 3c, we plotted the standard curve of the optimized one-pot assay using the point of inflection (POI), which is defined as the time corresponding to the maximum slope in the fluorescence intensity curve.[29,30] Although the fluorescence signals at low concentrations after 1 h were detectable, the significant uncertainty of iterative experiments indicate that the quantification at low concentrations may not be reliable. Due to the PEG crowding influence, the POI at low concentrations has visible standard deviations, resulting in poor sensitivity. The R^2 value was 0.921 from 10 cP/μL to 100 000 cP/μL, whereas it increased to 0.999 if the 10 cP/μL were not included in the calculation. Finally, we sought to verify the clinical performance of the one-pot assay by conducting a clinical validation to detect both HPV 16 and HPV 18 (Figure 3d). Among other sexually transmitted diseases (STD) including *Neisseria gonorrheae* (NG) and *Chlamydia trachomatis* (CT), the one-pot assay identified all clinical samples within 30 min, which is in 100% agreement with qPCR results (Tables S1 and S2).

Digital Quantification of the One-Pot CAs13a Assay by MEDICA. Similar to the standard-curve approach used in bulk PCR system, the aforementioned quantification based on POI shows obvious uncertainty at low concentrations (Figure 3c). Such a relative quantification method is sensitive to assay operating conditions and relies heavily on endogenous references or standards. The digital format of bulk assays (e.g., digital PCR[31]) has been proven to enable absolute quantification of the number of target molecules in individual partitions, where the assay takes place at the single-molecule level. Therefore, we converted the bulk reaction into digital quantification using droplet encapsulation. In addition, unlike the hot-start loop-mediated isothermal amplification (LAMP) and PCR,[23,33] RPA starts as soon as magnesium acetate (MgOAc) is added even at room temperature.[34,35] To avoid premature amplification before sample loading or partitioning,[36−38] we used a Y-shaped channel to separate MgOAc and the target-included master mix before loading them into the droplet generator (MEDICA). Thus, RPA is only triggered by MgOAc after droplet formation. The droplet digital assay contains three steps, droplet partition, droplet incubation, and digital visualization (Figure 4a). The mixture of MgOAc and target-included master mix was encapsulated into picoliter-sized water in oil droplets (~30 μm) (Figure S6). The resulting monodisperse emulsion droplets were incubated at 37 °C. After incubation, droplets were imaged by fluorescence microscopy and analyzed for the target concentration quantification.

We first evaluated the total reaction time of MEDICA. A customized stage was developed to capture the images of *in situ* MEDICA (Figure S7a). In the real-time MEDICA, we were able to detect significant fluorescence signals within 10 min when significant numbers of droplets are present (Figure S7b). We found the positive droplet ratio increased dramatically in 10−15 min and reached a plateau after 20 min (Figure 4b). In terms of the total fluorescence intensity, it increased until 25 min when the signals in droplets became saturated and where the amplification time (Cq) is between 5 and 10 min (Figure 4c). This indicates that the real-time MEDICA only took around 5−10 min for detection, which is more rapid than the corresponding assay in bulk solution. We postulated that this is because the RPA and Cas13a reactions are accelerated within a picoliter confined partition, and the signals generated are concentrated to facilitate the detection. The enhanced mobility of molecules in a less viscous fluid in droplets also contributes to the mixing of the reagents and therefore shortens the overall reaction time. Similar results have been reported in which the reaction in droplets is accelerated.[39,40]

Subsequently, we calibrated MEDICA by end-point quantification using serially diluted samples of synthetic HPV 16 plasmid. In each experiment, we used a sample of 20 μL to generate a total number of ~1.4 million droplets with a diameter of 30 μm. The results are shown in Figure 4d. The absence of the MgOAc group emitted even less fluorescence on average than the nontemplate control (NTC) group. The positive/negative droplets can be simply counted based on their end-point fluorescence using ImageJ and customized Matlab code, thanks to the background-free signals generated by Cas13a (Figure S8). Figure 4e shows that the highest intensity of the recorded droplets from the NTC group is less than 0.5 after normalization, while all the positive droplets were selected over 0.6. Thus, MEDICA enables near background-free digital quantification. The clear binary distribution of positive/negative droplets is attributed to the Cas13a detection system which utilizes specifically designed crRNA and collateral trans-cleavage for signal reporting. Moreover, the end-point fluorescence of the positive droplets appears more uniform with less interference of the rain droplets.[41] By tailoring the reporter concentration, the signal-to-background was steadily enhanced by increasing the reporting concentration (Figure S9), owing to the unique collateral cleavage of Cas13a.[42] Figure 4f shows the calibration curve of MEDICA for HPV 16 plasmid with a range of concentration from 1 to 10^6 copies/μL. Owing to the million

https://doi.org/10.1021/acs.analchem.2c00067
Anal. Chem. XXXX, XXX, XXX−XXX

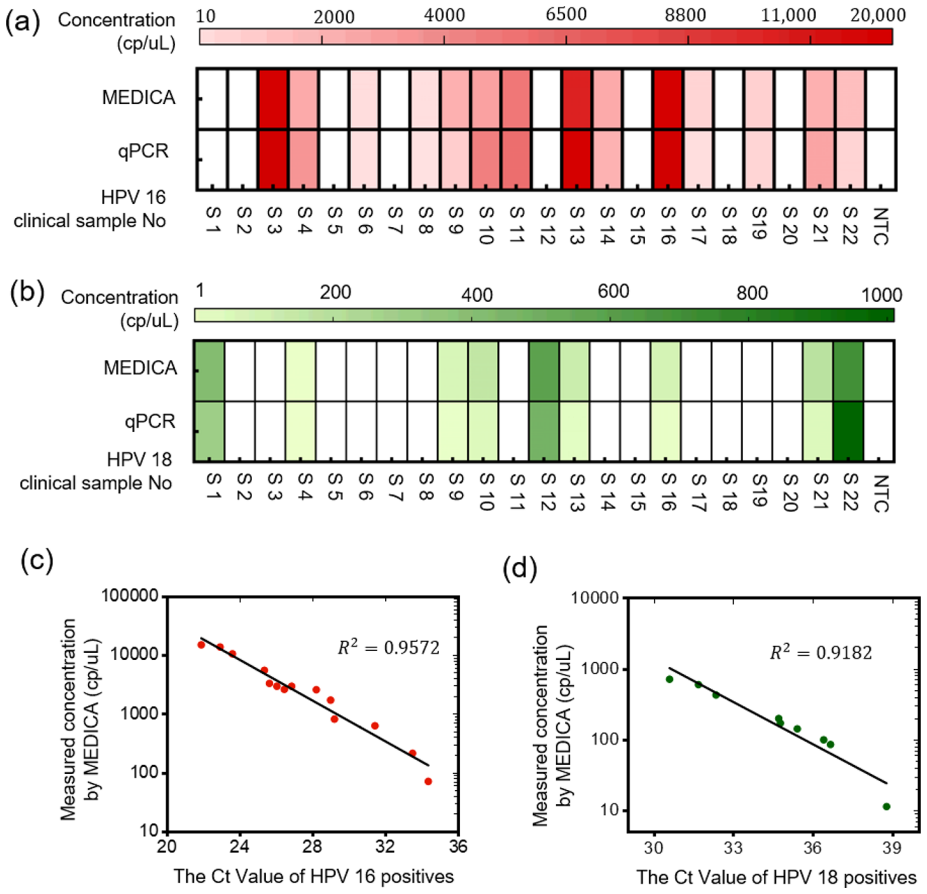


Figure 5. Clinical validation of MEDICA. (a) Comparison of MEDICA quantification results with qPCR results for detection of HPV 16. MEDICA identified all clinical samples with the same seemed of qPCR. (b) Comparison between MEDICA quantification results and qPCR quantification of HPV 18. (c) Correlation between the HPV 16 concentrations measured by MEDICA and the real-time qPCR C_t values. (d) Correlation between the HPV 18 concentrations measured by MEDICA and the real-time qPCR C_t values.

scale of the droplet partition number used in the digital quantification, the dynamic range is allowed to reach 6 orders of magnitude. We estimated the limit of detection (LOD) using $3\sigma/k$,[30] where σ is the standard deviation of the detected copy at 1 copy/μL and k is the slope of the calibration curve. The LOD was estimated as 1.1 copy/μL. Nevertheless, we cannot rule out the possible false negative cases due to the PEG crowding, droplet loss, or imaging issues.[32] Strategies including enhanced mixing in droplets, all-in-one device integration, and optimization of the one-pot reaction at single copy concentrations may further improve the sensitivity performance. We further tested the robustness of MEDICA to quantify HPV 18 E1, SARS-CoV-2 ORF, and N genes. We observed the equivalent linear correlation of all the groups (Figure 4g), which further indicated the versatility of MEDICA. Finally, we tested the selectivity of MEDICA in multiple conditions with or without the spiked samples. Taking HPV 16 as the main viral target, MEDICA successfully differentiated all the targets with consistent results (Figure 4h).

Clinical Validation of MEDICA. Finally, we demonstrated the feasibility of MEDICA to detect clinical viral HPV 16 and 18 samples. The typical sensitivity requirement of HPV detection is around 5 aM (10 cP/μL).[43] We conducted the absolute quantification using MEDICA (Figures S10 and S11) and the relative quantification using qPCR (Figure S12) for detection of HPV 16 and HPV 18 from 22 clinical samples. Both qPCR and MEDICA were able to detect all the positive viral HPV 16 and HPV 18 samples (Figure 5a,b). Since the C_t (threshold cycle) values straightforwardly represent the raw target concentration, we correlated the measured concentrations from MEDICA with the C_t values of qPCR (Tables S1 and S2) to verify the consistency of their results. The overall correlations of the measured C_t values and the quantified concentrations from MEDICA (Figure 5c,d) follow the expected trend. However, at the very low concentrations, the difference between these two methods tended to diverge. We believe these differences can be explained by three reasons. First, as the standard curves for qPCR were obtained using synthetic HPV plasmids, they may cause errors for the quantification of clinical samples, and qPCR has high uncertainty in quantification when the input copies are limited.[31] Second, the different targeting domains on the genome may cause differences due to the amplification efficiency. Third, the concentration of the clinical samples may change after several rounds of freeze−thaw. Overall, the clinical validation further confirms that MEDICA offers rapid, accurate, and direct quantification of nucleic acids from clinical specimens.

CONCLUSION

As an emerging diagnostic tool, the CRISPR-Cas system has demonstrated its excellence in nucleic acid rapid detection. To advance its potentiality in point-of-care testing, we addressed the bottleneck issues of the one-pot Cas13a assay including the

https://doi.org/10.1021/acs.analchem.2c00067
Anal. Chem. XXXX, XXX, XXX−XXX

viscous macromolecular crowding reaction and enzymatic incompatibility between RPA and Cas13a. Our optimized one-pot Cas13a counterpoises rapid, nonspecific RPA amplification with specific Cas13a detection. This method shows comparable performance with the two-step SHERLOCK method, which can be extended to facile dipstick tests or portable detection platforms. We further converted the developed assay for droplet digital quantification by MEDICA. By leveraging the droplet microfluidics, we arranged the resuspension of the sole MgOAc initiator and master mix, enabling the reaction to be triggered after droplets were formed. MEDICA achieves rapid and sensitive nucleic acid detection within 10 min and absolute quantification within 25 min, faster than other CRISPR-based diagnostic platforms such as SHERLOCK and SHINE (Table S3). Since the Cas13a system only triggers signals with the presence of desired targets, MEDICA achieves a uniform high signal-to-background ratio, enabling background-free end-point quantification. Because of its rapidity, sensitivity, specificity, and simple ancillary equipment, we expect that MEDICA holds great potential to be an isothermal alternative to PCR as the gold standard nucleic acid quantification.

■ ASSOCIATED CONTENT

Supporting Information

The Supporting Information is available free of charge at https://pubs.acs.org/doi/10.1021/acs.analchem.2c00067.

Figure S1, Coomassie-stained SDS-PAGE gel of protein fractions; Figure S2, two-step SHERLOCK Test and Cas13a collateral reporting test; Figure S3, construction of one-pot Cas13a reaction; Figure S4, comparison of initial one-pot reaction and optimized one-pot Cas13a reaction; Figure S5, sensitivity test for both HPV 16 and HPV 18; Figure S6, microfluidic chip design and droplet formation; Figure S7, real-time MEDICA; Figure S8, droplet fluorescence analysis; Figure S9, signal-to-background ratio versus the reporter concentration; Figure S10, end-point fluorescence images of MEDICA for detection of HPV 16 using 22 clinical samples and NTC; Figure S11, end-point fluorescence images of MEDICA for detection of HPV 18 using 22 clinical samples and NTC; Figure S12, qPCR clinical test; Table S1, C_t values of qPCR for detection of HPV16 using clinical samples; Table S2, C_t values of qPCR for detection of HPV18 using clinical samples; Table S3, comparison of MEDICA with other CRISPR nucleic acid detection methods; Table S4, chemicals used in this work; and Table S5, sequences used in this work (PDF)

■ AUTHOR INFORMATION

Corresponding Authors

Ben Zhong Tang − *Department of Chemical and Biological Engineering and Department of Chemistry, Hong Kong Branch of Chinese National Engineering Research Center for Tissue Restoration and Reconstruction, The Hong Kong University of Science and Technology, Kowloon 999077, Hong Kong; Shenzhen Institute of Molecular Aggregate Science and Engineering, School of Science and Engineering, The Chinese University of Hong Kong, Shenzhen, Shenzhen City, Guangdong 518172, China;* orcid.org/0000-0002-0293-964X; Email: tangbenz@ust.hk

Shuhuai Yao − *Department of Mechanical and Aerospace Engineering, The Hong Kong University of Science and Technology, Kowloon 999077, Hong Kong; Department of Chemical and Biological Engineering, The Hong Kong University of Science and Technology, Kowloon 999077, Hong Kong;* orcid.org/0000-0001-7059-4092; Email: meshyao@ust.hk

Authors

Frank X. Liu − *Department of Mechanical and Aerospace Engineering, The Hong Kong University of Science and Technology, Kowloon 999077, Hong Kong*

Johnson Q. Cui − *Department of Mechanical and Aerospace Engineering, The Hong Kong University of Science and Technology, Kowloon 999077, Hong Kong*

Hojeong Park − *Department of Chemical and Biological Engineering and Department of Chemistry, Hong Kong Branch of Chinese National Engineering Research Center for Tissue Restoration and Reconstruction, The Hong Kong University of Science and Technology, Kowloon 999077, Hong Kong;* orcid.org/0000-0001-7820-4271

Ka Wai Chan − *DiagCor Life Science Limited, Kowloon 999077, Hong Kong*

Tyler Leung − *DiagCor Life Science Limited, Kowloon 999077, Hong Kong*

Complete contact information is available at: https://pubs.acs.org/10.1021/acs.analchem.2c00067

Author Contributions

¶F.X.L., J.Q.C., and H.P. contributed equally to this work.

Notes

The authors declare no competing financial interest.

■ ACKNOWLEDGMENTS

We would like to thank HKUST NFF for microfluidic chip fabrication and HKUST BioCRF for the essential equipment support. This work is supported by the University-Industry Collaboration Programme (Grant No. UIM/362) under the Innovation and Technology Fund of Hong Kong.

■ REFERENCES

(1) Wang, C.; Horby, P. W.; Hayden, F. G.; Gao, G. F. *lancet* **2020**, *395*, 470−473.

(2) Vogels, C. B. F.; Brito, A. F.; Wyllie, A. L.; Fauver, J. R.; Ott, I. M.; Kalinich, C. C.; Petrone, M. E.; Casanovas-Massana, A.; Catherine Muenker, M.; Moore, A. J.; Klein, J.; Lu, P.; Lu-Culligan, A.; Jiang, X.; Kim, D. J.; Kudo, E.; Mao, T.; Moriyama, M.; Oh, J. E.; Park, A.; Silva, J.; Song, E.; Takahashi, T.; Taura, M.; Tokuyama, M.; Venkataraman, A.; Weizman, O.-E.; Wong, P.; Yang, Y.; Cheemarla, N. R.; White, E. B.; Lapidus, S.; Earnest, R.; Geng, B.; Vijayakumar, P.; Odio, C.; Fournier, J.; Bermejo, S.; Farhadian, S.; Dela Cruz, C. S.; Iwasaki, A.; Ko, A. I.; Landry, M. L.; Foxman, E. F.; Grubaugh, N. D. *Nat. Microbiol.* **2020**, *5*, 1299−1305.

(3) Yang, Q.; Saldi, T. K.; Gonzales, P. K.; Lasda, E.; Decker, C. J.; Tat, K. L.; Fink, M. R.; Hager, C. R.; Davis, J. C.; Ozeroff, C. D.; Muhlrad, D.; Clark, S. K.; Fattor, W. T.; Meyerson, N. R.; Paige, C. L.; Gilchrist, A. R.; Barbachano-Guerrero, A.; Worden-Sapper, E. R.; Wu, S. S.; Brisson, G. R.; McQueen, M. B.; Dowell, R. D.; Leinwand, L.; Parker, R.; Sawyer, S. L. *Proc. Natl. Acad. Sci. U. S. A.* **2021**, *118*, e2104547118.

(4) Ackerman, C. M.; Myhrvold, C.; Thakku, S. G.; Freije, C. A.; Metsky, H. C.; Yang, D. K.; Ye, S. H.; Boehm, C. K.; Kosoko-Thoroddsen, T.-S. F.; Kehe, J.; Nguyen, T. G.; Carter, A.; Kulesa, A.; Barnes, J. R.; Dugan, V. G.; Hung, D. T.; Blainey, P. C.; Sabeti, P. C. *Nature* **2020**, *582*, 277−282.

(5) Barnes, K. G.; Lachenauer, A. E.; Nitido, A.; Siddiqui, S.; Gross, R.; Beitzel, B.; Siddle, K. J.; Freije, C. A.; Dighero-Kemp, B.; Mehta, S. B.; Carter, A.; Uwanibe, J.; Ajogbasile, F.; Olumade, T.; Odia, I.; Sandi, J. D.; Momoh, M.; Metsky, H. C.; Boehm, C. K.; Lin, A. E.; Kemball, M.; Park, D. J.; Branco, L.; Boisen, M.; Sullivan, B.; Amare, M. F.; Tiamiyu, A. B.; Parker, Z. F.; Iroezindu, M.; Grant, D. S.; Modjarrad, K.; Myhrvold, C.; Garry, R. F.; Palacios, G.; Hensley, L. E.; Schaffner, S. F.; Happi, C. T.; Colubri, A.; Sabeti, P. C. *Nat. Commun.* **2020**, *11*, 4131.
(6) Broughton, J. P.; Deng, X.; Yu, G.; Fasching, C. L.; Servellita, V.; Singh, J.; Miao, X.; Streithorst, J. A.; Granados, A.; Sotomayor-Gonzalez, A.; Zorn, K.; Gopez, A.; Hsu, E.; Gu, W.; Miller, S.; Pan, C.-Y.; Guevara, H.; Wadford, D. A.; Chen, J. S.; Chiu, C. Y. *Nat. Biotechnol.* **2020**, *38*, 870−874.
(7) Ding, X.; Yin, K.; Li, Z.; Lalla, R. V.; Ballesteros, E.; Sfeir, M. M.; Liu, C. *Nat. Commun.* **2020**, *11*, 4711.
(8) Gootenberg, J. S.; Abudayyeh, O. O.; Kellner, M. J.; Joung, J.; Collins, J. J.; Zhang, F. *Science* **2018**, *360*, 439−444.
(9) Joung, J.; Ladha, A.; Saito, M.; Kim, N.-G.; Woolley, A. E.; Segel, M.; Barretto, R. P.J.; Ranu, A.; Macrae, R. K.; Faure, G.; Ioannidi, E. I.; Krajeski, R. N.; Bruneau, R.; Huang, M.-L. W.; Yu, X. G.; Li, J. Z.; Walker, B. D.; Hung, D. T.; Greninger, A. L.; Jerome, K. R.; Gootenberg, J. S.; Abudayyeh, O. O.; Zhang, F. *N. Engl. J. Med.* **2020**, *383*, 1492−1494.
(10) Patchsung, M.; Jantarug, K.; Pattama, A.; Aphicho, K.; Suraritdechachai, S.; Meesawat, P.; Sappakhaw, K.; Leelahakorn, N.; Ruenkam, T.; Wongsatit, T.; Athipanyasilp, N.; Eiamthong, B.; Lakkanasirorat, B.; Phoodokmai, T.; Niljianskul, N.; Pakotiprapha, D.; Chanarat, S.; Homchan, A.; Tinikul, R.; Kamutira, P.; Phiwkaow, K.; Soithongcharoen, S.; Kantiwiriyawanitch, C.; Pongsupasa, V.; Trisrivirat, D.; Jaroensuk, J.; Wongnate, T.; Maenpuen, S.; Chaiyen, P.; Kamnerdnakta, S.; Swangsri, J.; Chuthapisith, S.; Sirivatanauksorn, Y.; Chaimayo, C.; Sutthent, R.; Kantakamalakul, W.; Joung, J.; Ladha, A.; Jin, X.; Gootenberg, J. S.; Abudayyeh, O. O.; Zhang, F.; Horthongkham, N.; Uttamapinant, C. *Nat. Biomed. Eng.* **2020**, *4*, 1140−1149.
(11) Knott, G. J.; Doudna, J. A. *Science* **2018**, *361*, 866−869.
(12) Chertow, D. S. *Science* **2018**, *360*, 381−382.
(13) Gootenberg, J. S.; Abudayyeh, O. O.; Lee, J. W.; Essletzbichler, P.; Dy, A. J.; Joung, J.; Verdine, V.; Donghia, N.; Daringer, N. M.; Freije, C. A.; Myhrvold, C.; Bhattacharyya, R. P.; Livny, J.; Regev, A.; Koonin, E. V.; Hung, D. T.; Sabeti, P. C.; Collins, J. J.; Zhang, F. *Science* **2017**, *356*, 438−442.
(14) Chen, J. S.; Ma, E.; Harrington, L. B.; Da Costa, M.; Tian, X.; Palefsky, J. M.; Doudna, J. A. *Science* **2018**, *360*, 436−439.
(15) Ramachandran, A.; Santiago, J. G. *Anal. Chem.* **2021**, *93*, 7456.
(16) East-Seletsky, A.; O'Connell, M. R.; Burstein, D.; Knott, G. J.; Doudna, J. A. *Mol. Cell* **2017**, *66*, 373−383.e3.
(17) Myhrvold, C.; Freije, C. A.; Gootenberg, J. S.; Abudayyeh, O. O.; Metsky, H. C.; Durbin, A. F.; Kellner, M. J.; Tan, A. L.; Paul, L. M.; Parham, L. A.; Garcia, K. F.; Barnes, K. G.; Chak, B.; Mondini, A.; Nogueira, M. L.; Isern, S.; Michael, S. F.; Lorenzana, I.; Yozwiak, N. L.; MacInnis, B. L.; Bosch, I.; Gehrke, L.; Zhang, F.; Sabeti, P. C. *Science* **2018**, *360*, 444−448.
(18) Arizti-Sanz, J.; Freije, C. A.; Stanton, A. C.; Petros, B. A.; Boehm, C. K.; Siddiqui, S.; Shaw, B. M.; Adams, G.; Kosoko-Thoroddsen, T.-S. F.; Kemball, M. E.; Uwanibe, J. N.; Ajogbasile, F. V.; Eromon, P. E.; Gross, R.; Wronka, L.; Caviness, K.; Hensley, L. E.; Bergman, N. H.; MacInnis, B. L.; Happi, C. T.; Lemieux, J. E.; Sabeti, P. C.; Myhrvold, C. *Nat. Commun.* **2020**, *11*, 5921.
(19) Taylor, S. C.; Carbonneau, J.; Shelton, D. N.; Boivin, G. *J. Virol. Methods* **2015**, *224*, 58−66.
(20) Salipante, S. J.; Jerome, K. R. *Clin.Chem.* **2020**, *66*, 117−123.
(21) Kaminski, M. M.; Abudayyeh, O. O.; Gootenberg, J. S.; Zhang, F.; Collins, J. J. *Nature Biomedical Engineering* **2021**, *5*, 643−656.
(22) Kellner, M. J.; Koob, J. G.; Gootenberg, J. S.; Abudayyeh, O. O.; Zhang, F. *Nature protocols* **2019**, *14*, 2986−3012.
(23) Piepenburg, O.; Williams, C. H.; Stemple, D. L.; Armes, N. A. *PLoS Biol.* **2006**, *4*, e204.
(24) Zimmerman, S. B.; Harrison, B. *Proc. Natl. Acad. Sci. U. S. A.* **1987**, *84*, 1871−1875.
(25) Ellis, R. J. *Trends Biochem. Sci.* **2001**, *26*, 597−604.
(26) Lillis, L.; Siverson, J.; Lee, A.; Cantera, J.; Parker, M.; Piepenburg, O.; Lehman, D. A.; Boyle, D. S. *Mol.Cell.Probes.* **2016**, *30*, 74−78.
(27) Woodman, C. B.; Collins, S. I.; Young, L. S. *Nature Reviews Cancer* **2007**, *7*, 11−22.
(28) Baret, J. *Lab Chip* **2012**, *12*, 422−433.
(29) Shi, C.; Shang, F.; Pan, M.; Liu, S.; Ma, C. *Biosens. Bioelectron.* **2016**, *80*, 54−58.
(30) Huang, M.; Zhou, X.; Wang, H.; Xing, D. *Anal. Chem.* **2018**, *90*, 2193−2200.
(31) Hindson, C. M.; Chevillet, J. R.; Briggs, H. A.; Gallichotte, E. N.; Ruf, I. K.; Hindson, B. J.; Vessella, R. L.; Tewari, M. *Nat. Methods* **2013**, *10*, 1003−1005.
(32) Chen, L.; Yadav, V.; Zhang, C.; Huo, X.; Wang, C.; Senapati, S.; Chang, H. *Anal. Chem.* **2021**, *93*, 6456−6462.
(33) Zhao, Y.; Chen, F.; Li, Q.; Wang, L.; Fan, C. *Chem. Rev.* **2015**, *115*, 12491−12545.
(34) Yeh, E.; Fu, C.; Hu, L.; Thakur, R.; Feng, J.; Lee, L. P. *Sci. Adv.* **2017**, *3*, e1501645.
(35) Li, J.; Macdonald, J.; von Stetten, F. *Analyst* **2019**, *144*, 31−67.
(36) Park, J. S.; Hsieh, K.; Chen, L.; Kaushik, A.; Trick, A. Y.; Wang, T. *Advanced Science* **2021**, *8*, 2003564.
(37) Tian, T.; Shu, B.; Jiang, Y.; Ye, M.; Liu, L.; Guo, Z.; Han, Z.; Wang, Z.; Zhou, X. *ACS Nano* **2021**, *15*, 1167.
(38) Wu, X.; Tay, J. K.; Goh, C. K.; Chan, C.; Lee, Y. H.; Springs, S. L.; Wang, D. Y.; Loh, K. S.; Lu, T. K.; Yu, H. *Biomaterials* **2021**, *274*, 120876.
(39) Kalsi, S.; Valiadi, M.; Tsaloglou, M.-N.; Parry-Jones, L.; Jacobs, A.; Watson, R.; Turner, C.; Amos, R.; Hadwen, B.; Buse, J.; Brown, C.; Sutton, M.; Morgan, H. *Lab Chip* **2015**, *15*, 3065−3075.
(40) Gines, G.; Menezes, R.; Nara, K.; Kirstetter, A.; Taly, V.; Rondelez, Y. *Sci. Adv.* **2020**, *6*, eaay5952.
(41) Trypsteen, W.; Vynck, M.; De Neve, J.; Bonczkowski, P.; Kiselinova, M.; Malatinkova, E.; Vervisch, K.; Thas, O.; Vandekerckhove, L.; De Spiegelaere, W. *Anal. Bioanal. Chem.* **2015**, *407*, 5827−5834.
(42) Cui, J. Q.; Liu, F. X.; Park, H.; Chan, K. W.; Leung, T.; Tang, B. Z.; Yao, S. *Biosens. Bioelectron.* **2022**, *202*, 114019.
(43) Moberg, M.; Gustavsson, I.; Gyllensten, U. *J. Clin. Microbiol.* **2003**, *41*, 3221−3228.

https://doi.org/10.1021/acs.analchem.2c00067
Anal. Chem. XXXX, XXX, XXX−XXX